
Mechanical Engineering Faculty Publications

Mechanical Engineering Department

2-2009

On Stresses Induced in a Thermal Barrier Coating Due to Indentation Testing


Jin Yan
University of Delaware

Anette M. Karlsson
Cleveland State University, a.karlsson@csuohio.edu

Marion Bartsch
German Aerospace Center

Xi Chen
Columbia University

Follow this and additional works at: https://engagedscholarship.csuohio.edu/enme_facpub

 Part of the [Materials Science and Engineering Commons](#), and the [Mechanical Engineering Commons](#)
How does access to this work benefit you? Let us know!

Original Citation

Yan, J., Karlsson, A. M., Bartsch, M., 2009, "On Stresses Induced in a Thermal Barrier Coating due to Indentation Testing," *Computational Materials Science*, 44(4) pp. 1178-1191.

This Article is brought to you for free and open access by the Mechanical Engineering Department at EngagedScholarship@CSU. It has been accepted for inclusion in Mechanical Engineering Faculty Publications by an authorized administrator of EngagedScholarship@CSU. For more information, please contact library.es@csuohio.edu.

On stresses induced in a thermal barrier coating due to indentation testing

Jin Yan^a, Anette M. Karlsson^{a,*}, Marion Bartsch^b, Xi Chen^c

^a Department of Mechanical Engineering, University of Delaware, Newark, DE 19716, USA

^b Institute of Materials Research, German Aerospace Center (DLR), Linder Hoehe, D-51147 Cologne, Germany

^c Department of Civil Engineering and Engineering Mechanics, Columbia University, New York, NY 10027-6699, USA

1. Introduction

Thermal barrier coatings (TBCs) are multilayered coatings that are frequently used in gas turbine applications to protect structural components from the intrinsic high temperatures. By actively cooling the structural component, the TBC can sustain a temperature difference of up to 150 °C during use. Thus, the thermal load on the structural component is reduced, and it is possible to either operate the turbine at higher temperature or increase the life time of the structural component. Unfortunately, the coatings fail prematurely, preventing the benefits of TBCs to be fully utilized. Even though there are several possible scenarios that eventually can lead to the failure of a TBC, a dominating class of failure is associated with nucleation of damage at or near an interface, followed by crack growth and coalescence parallel to the interface, resulting in that the coating eventually spalls from the substrate. Thus, interfacial damage increases with use (i.e., the age) of the system. Consequently, several authors have suggested that the interfacial fracture toughness could be a measure describing how damage accumulates in the TBC as the system is aged [1–5]. However, there

is currently no consensus on how to measure the interfacial fracture toughness of TBCs [4,6,7].

The challenges associated with designing and testing TBCs comes from the multilayered structure of the coating, where the properties evolve as the system is used. For the TBC systems considered here, three major layers can be identified, starting from the substrate (Fig. 1): (i) a metallic bond coat; (ii) a thermally grown oxide (TGO); and (iii) a ceramic top coat. Currently, the most common top coat is yttria stabilized zirconia (YSZ). There are two major groups of bond coats: platinum modified aluminide and MCrAlY (where M stands for iron (Fe) or nickel and cobalt (NiCo)). The TGO is a reaction product that is formed during high temperature exposure. Currently, the preferred TGO is α -alumina, which is formed by that the bond coat provides aluminum and from the oxygen that diffuses through the YSZ, which is permeable to oxygen. However, the TGO commonly also has other oxidation products that may affect the overall interfacial strength, e.g., Ref. [8].

Several methods have been proposed to measure the interfacial fracture toughness of thermal barrier coatings, including "pull-out techniques" (an extension of methods used for testing fibers in a ceramic or metal matrix) [9], notched coatings in 4-point bending [10], and various indentation techniques [4,6,7,11,12]. The indentation technique has been proposed by many as the most promising method, since it is easy to perform and involves minimum

* Corresponding author. Fax: +1 302 831 3619.

E-mail address: karlsson@udel.edu (A.M. Karlsson).

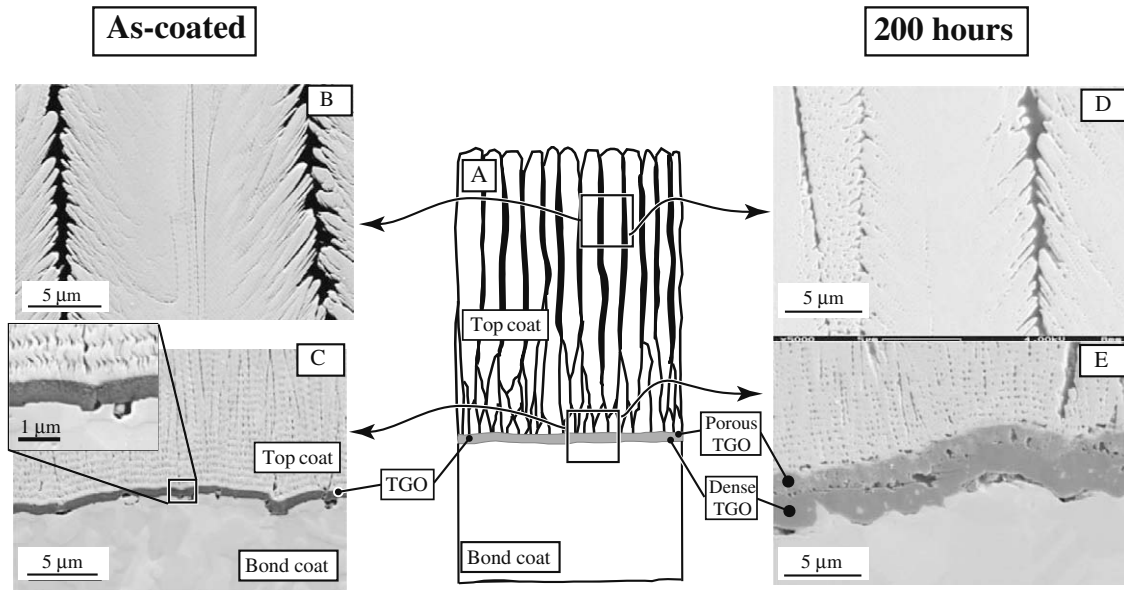


Fig. 1. Schematic and SEM images of the thermal barrier system, showing as-coated samples and samples aged for 200 h at 1000 °C in air. The as-coated sample shows (B) the intercolumnar spacing (ICS) between YSZ columns near the top coat surface and (C) the intermixed, porous (preexisting) TGO. The aged samples show (D) narrowed ICS and rigid connections between the YSZ columns and (E) the bi-layered structure of the TGO. For both as-coated and aged samples, the top coat closest to the TGO does not show expressed ICS between columns.

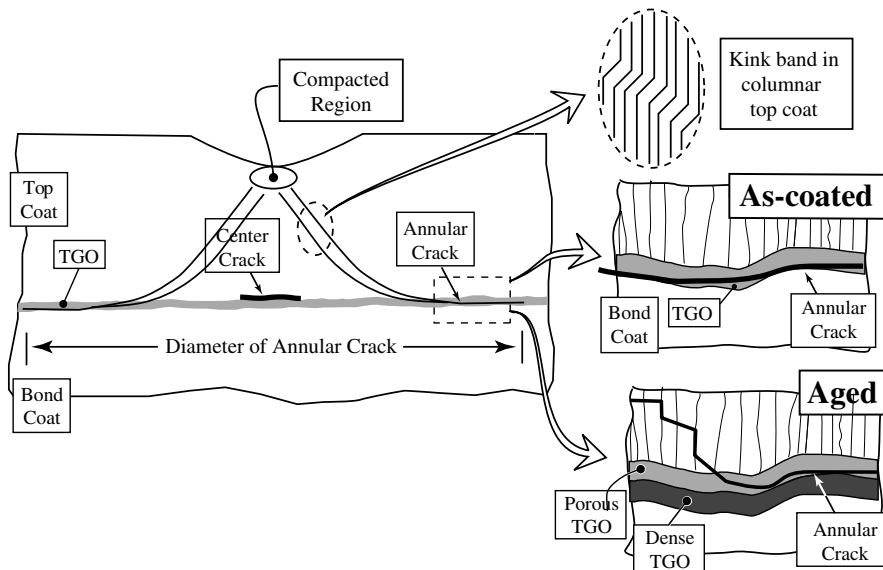


Fig. 2. Schematic of the main pattern after indentation, including the kink-bands. The extended annular delamination crack tends to propagate in the TGO and TGO-bond coat interface for as-coated samples but does not reach the bond coat interface for the aged samples.

sample preparation. However, as was shown in our previous work, the results may be hard to interpret since they are indirectly associated with material toughness (not just interfacial toughness) and deformation modes, and may even give contradicting results [6,7].

In our experimental work, we investigated Rockwell indentation of thermal barrier coatings, where the indentation was conducted on the surface of a thermal barrier system so to establish the interfacial fracture toughness [6]. Two classes of TBCs systems were investigated: one set was tested in “as-coated” conditions and the second set had been subjected to thermal heat treatment. Based on previous observations, e.g., Refs. [1–4], it was expected that the heat treated (aged) samples should exhibit lower interfa-

cial toughness than the as-coated and that the delamination size would increase with increasing maximum indentation load. However, the results indicated otherwise. These contradictive results will be explored here by means of finite element simulations. In the following, we first summarize the experimental results, before discussing the finite element models and the results.

2. Experimental investigations

The experimental work and results were discussed in Ref. [6], and will be summarized here for clarity.

2.1. Specimens and experimental procedures

Flat specimens of IN 625 and a limited number of CMSX-4 were coated by electron beam physical vapor deposition (EB-PVD), first with a NiCoCrAlY bond coat (100 μm) followed by a partially stabilized YSZ (7–8 wt% yttria, 280 μm). Before indentation testing, thermal aging was conducted, where a set of samples was subjected to 1000 $^{\circ}\text{C}$ in air for 50, 100, 200, and 400 h, respectively. The samples were kept at high temperature for 23 h and at room temperature for 1 h, until the specified “time-at-temperature” was reached. Spontaneous spallation occurred in the samples aged to 400 h; consequently, these were not used in the indentation testing. The samples aged for 200 h were indented, but showed delayed spontaneous spallation after indentation (“desk-top failure”). Thus, only limited evaluation could be done for the 200 h samples. The behavior of all aged specimens was compared to specimens that were not heat treated, i.e., tested in “as-coated” conditions.

An electromechanical testing machine was used to indent the coated surface with a Rockwell brale C indenter [6]. During the indentation testing, the indentation displacement and force were recorded continuously. In some cases, the pre-selected maximum indentation force was not exactly achieved since the equipment was manually controlled. Several indentations could be made on each sample, where each indentation imprint was separated with at least 10 mm to avoid interference between the stress fields generated.

A key part of the experimental investigations was to investigate the damage in the TBC after the indentation, thus careful sample preparation for microscopy was conducted. A detailed description of the procedure is presented in Ref. [6]. The specimens were analyzed by both an optical microscope and a scanning electron microscope.

2.2. Experimental observations

The heat treatment of the samples causes changes in the microstructures, including sintering of the YSZ and growth of the TGO, as illustrated in Fig. 1 [6]. The sintering of the top coat is associated with that the featherlike structure of the columnar YSZ and the pores gets coarser, along with the formation of rigid contacts between the columns. The TGO grows from a single intermixed oxide layer in the as-coated samples to a bi-layered TGO, which includes the preexisting TGO along with a newly grown, dense TGO, Fig. 1. The intermixed layer consists of both aluminum oxide and zirconia, in accordance with previous observations of the selected material system [8].

The microstructural imaging of cross-sections of the indented regions indicated that there are three major classes of damage induced by the Rockwell indentation,¹ Fig. 2: (i) crushing of the top coat adjacent to the indenter tip; (ii) cone shaped shear bands; and (iii) interfacial debonding cracks. The interfacial debonding cracks are found in the vicinity of the TGO, but not necessarily at a particular interface. An “overall debonding crack” typically starts from the cone-crack, kinks when it reaches the interface, and becomes parallel to the TGO, propagating in the YSZ. As the crack grows further from the center of the indentation, the crack propagates into the TGO. In the as-coated samples, the annular debonding crack eventually propagates in the TGO and the TGO–bond coat interface. However, for the aged samples, the TGO cracks were not able to propagate through the dense (and new) TGO, Fig. 2. For indentation forces larger than 200 N, the substrate and bond coat

yields, resulting in permanent deformations not only in the top coat, but also of the underlying layers [6].

To investigate if the indentation technique indeed can be used as a test method for determining interfacial fracture toughness in a thermal barrier coating, the diameter of the delamination crack was measured in the SEM (Fig. 3). For smaller loads and aged samples, the delamination size sometimes coincides with the cone-crack diameter. Even though some scatter is observed, two distinct regions are identified: a bifurcating in the behavior can be seen for indentation forces around 175 N. By using a linear curve fit based on linear regression, an estimate of the delamination diameter as a function of maximum indentation force is obtained, Fig. 3. Based on these curves, it appears that there is one type of response for lower indentation forces and another for higher indentation forces, where the lower maximum indentation forces result in a higher slope (of the delamination–indentation force curve) than for the higher maximum indentation forces. For the lower loads, a minor but distinct difference can be seen between the as-coated and the aged samples (Fig 3B). For the higher maximum indentation forces, the as-coated specimens result in significantly larger

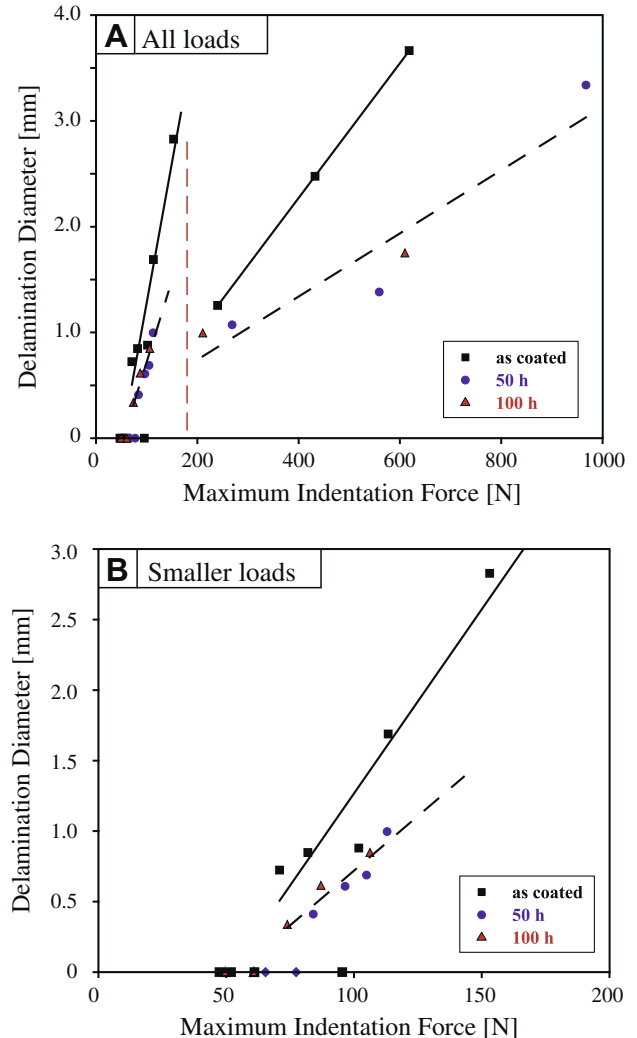


Fig. 3. The diameter of the annular delamination cracks as a function of the maximum indentation force. Linear regressions for as-coated samples are shown with solid lines and for aged samples with dashed lines (there is no statistical difference between 50 h and 100 h samples). The delamination diameter show two distinct responses: one for small maximum indentation forces and one for larger maximum indentation forces, with a bifurcation around 175 N. (The diameter is measured after unloading.) (A) All loads and (B) enlargement for smaller loads.

¹ Due to the scale of the indentation, the radius of the tip of the Rockwell indenter has to be considered.

delamination than the aged samples (Fig. 3A). This is a contradiction to what is observed in durability experiments and in field tests of thermal barrier coatings [5,13].

This study attempts to explain some of these observations through numerical simulations.

3. Numerical model

Numerical simulations using finite element analysis (FEA) is employed to investigate the micro-mechanical response in the TBC due to indentation. We will limit the discussion to the stress

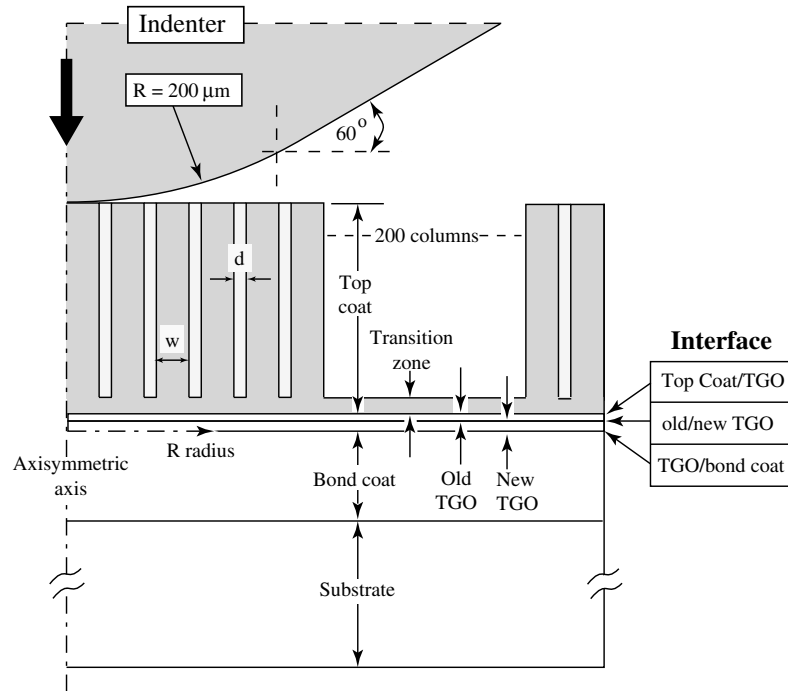


Fig. 4. Schematic of the axis-symmetric model with columnar top coat including the intercolumnar spacing (ICS), d . The radius of the indenter tip is included in the model. (The standard Rockwell brale C indenter as used in the test has a tip radius of 0.2 mm.)

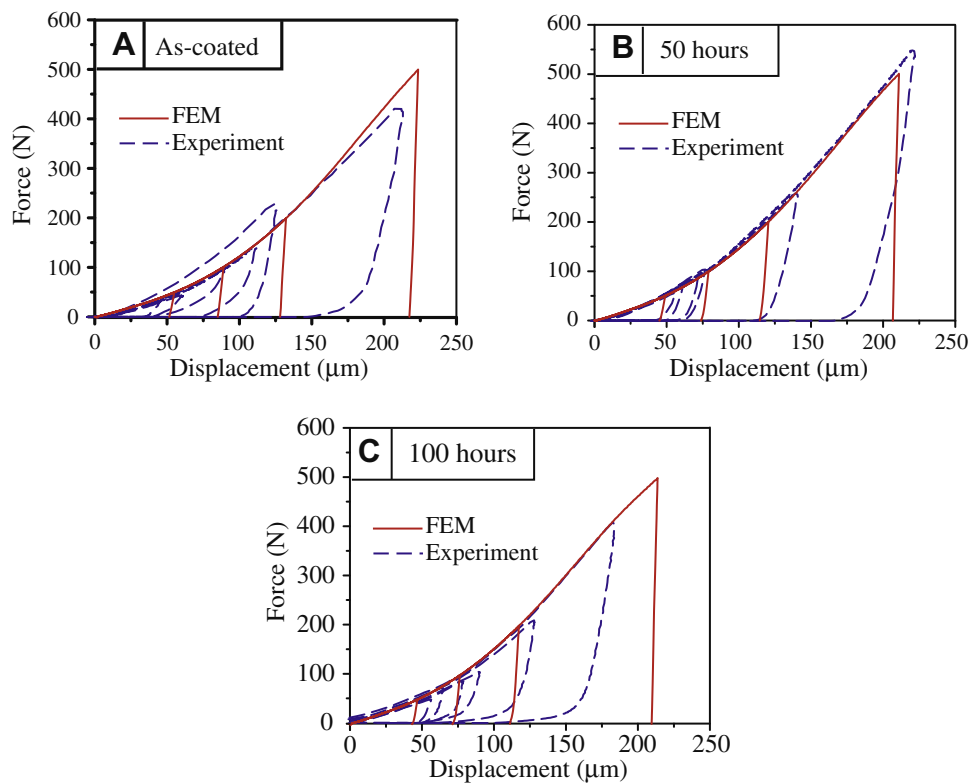


Fig. 5. Force-displacement curves from experiments and numerical simulation of the columnar structure: (A) as-coated, (B) 50 h aged, (C) 100 h aged.

Table 1
Geometry of the columnar model (ICS, intercolumnar spacing, Fig. 4)

	Column height (μm)	Column width (μm)	ICS width (μm)	Transition zone (μm)	Preexisting TGO thickness (μm)	New TGO thickness (μm)	BC thickness (μm)	Substrate thickness (μm)
As-coated	300	9.0	1.0	8.0	2.0	0	96	3000
Aged 50 h	300	9.2	0.8	8.0	2.0	2.0	94	3000
Aged 100 h	300	9.5	0.5	8.0	2.0	4.0	92	3000

fields generated during the indentation process: during loading, at maximum load, during unloading, and after complete unloading. This will give a qualitative assessment of the likely failure evolution while keeping the computational scheme tractable. The commercial available code ABAQUS [14] is used on Intel based work stations. The Rockwell indenter is simulated using the option of “rigid contact surface” in ABAQUS [14]. Since the tip of the indenter was not a perfectly sharp point in the experiment, the radius of the indenter tip is incorporated, as indicated in Fig. 4.² Large deformations and strains were assumed in the simulations, incorporated by using the option of “non-linear geometry” [14]. Axi-symmetric geometry was assumed.

Two classes of models are used to simulate the top coat. First, a homogeneous material is assumed, where the top coat is given properties corresponding to a porous media. In the second class of model, a columnar structure is assumed, Fig. 4. The model used for the columnar structure is based on an adoption of previous models used for simulating “foreign object damage” (when small particles that are present in the hot gas impact the top coat surface) [15] and “CMAS” (where particles that are present in the hot gas are deposited and melt into the columnar top coat during high temperature operation) [16]. The porous media is modeled with “Gurson’s porous metal plasticity theory” including void nucleation [17], as defined in ABAQUS [14]. This yield condition is a function of the volume fraction of the voids, f_0 . During heat treatment, the top coat sinters and consequently the relative density, $\bar{\rho} = 1 - f_0$, of the top coat increases. Hence, to simulate aging, the relative density was increased and is discussed later in this section.

For both models, CAX4R 4-node elements were used, with more than 24,000 elements. Comparisons with a model having a significant denser mesh (more than 85,000 elements) were performed, and since the denser model gave the same result as the coarser, we use the coarser mesh to save computational time. The two geometric configurations considered (the homogeneous top coat and the columnar top coat) have the same number of elements, but the distribution of elements over the layers (top coat, TGO, and bond coat) is different. In the case of a homogeneous top coat, all elements in one particular layer (i.e., top coat, TGO or bond coat) are assigned one set of material properties, respectively. However, in the model with a columnar structure, the top coat is divided into two parts: columns and the intercolumnar spacing (ICS), (i.e., a region of low density material between the major columnar features, Fig. 1), Fig. 4. The elements in the columns are assigned to properties of porous YSZ, and the elements simulating the ICS are defined as highly porous YSZ. Between the contact surfaces of the indenter and the top coat, Coulomb’s law of friction is assumed, with the coefficient of friction set to 0.5. (The coefficient of friction has only minor influence in indentation according to Ref. [18].)

In both models the interface between the TGO and top coat is modeled by a $6\ \mu\text{m}$ transition zone of YSZ. This layer simulates an YSZ with higher density, which corresponds to the initial deposition of the top coat (Fig. 1) before the columnar structure with expressed ICS has developed. The thickness of the transition zone is kept constant during aging.

Aging of the system is simulated by changing three classes of parameters:

- (i) Increasing the width of the columns in the top coat and (consequently) decreasing the distance (ICS) between the columns. This simulates the sintering effect as discussed in Fig. 1. The selected geometry is presented in Table 1.
- (ii) Increasing the thickness of the TGO, combined with decreasing the thickness of bond coat. This simulates the new TGO that forms at elevated temperatures on the expense of the aluminum diffusing through the bond coat. Table 1 summarizes the associated geometry change and Table 2 the material properties used.
- (iii) Changing the material properties of the top coat, including the relative density of the columnar top coat and intercolumnar materials, discussed below.

The properties of the top coat were determined by performing virtual indentation tests for a range of properties and comparing to the experimental data. The simulations are most sensitive for the volume fraction of voids, f_0 . By varying this value, along with the elastic modulus for both for the material simulating the highly porous intercolumnar spacing (ICS) and the columns, suitable material combination for the various aged systems were established. The selected material properties are shown in Table 2. For simplicity, the ICS is assumed elastic, with a very low elastic modulus. The numerically obtained force-displacement curves show excellent agreement to the experimental data during loading, Fig. 5. However, the unloading curves do not match as well as the loading curves. For all cases, the numerical simulations give significantly “stiffer” response than the experiments (i.e., the unloading in the numerical model gives a steeper unloading curve than the experimental data). We believe this is caused by that during unloading, cracks develop (as will be discussed later) in the experiment. However, in the current model, we do not consider the crack initiation and propagation, making the model stiffer than the real test.

Table 2
Material properties for the top coat (columns and intercolumnar spacing, ICS) and TGO (as-coated and new)

	Top coat columns	ICS in top coat	Preexisting TGO	New TGO
<i>As-coated</i>				
Elastic modulus, E (GPa)	70.0	0.8	300.0	–
Yield strength, σ_y (MPa)	500.0	–	600.0	–
Relative density, $\bar{\rho} = 1 - f_0$	0.8	0.4	0.9	–
<i>Aged 50 h</i>				
Elastic modulus, E (GPa)	75.0	0.9	300.0	380.0
Yield strength, σ_y (MPa)	500.0	–	600.0	700
Relative density, $\bar{\rho} = 1 - f_0$	0.85	0.6	0.9	–
<i>Aged 100 h</i>				
Elastic modulus, E (GPa)	80.0	1.0	300.0	380.0
Yield strength, σ_y (MPa)	500.0	–	600.0	700
Relative density, $\bar{\rho} = 1 - f_0$	0.9	0.8	0.9	–

² The radius of a Rockwell Brale C indenter tip is 0.2 mm.

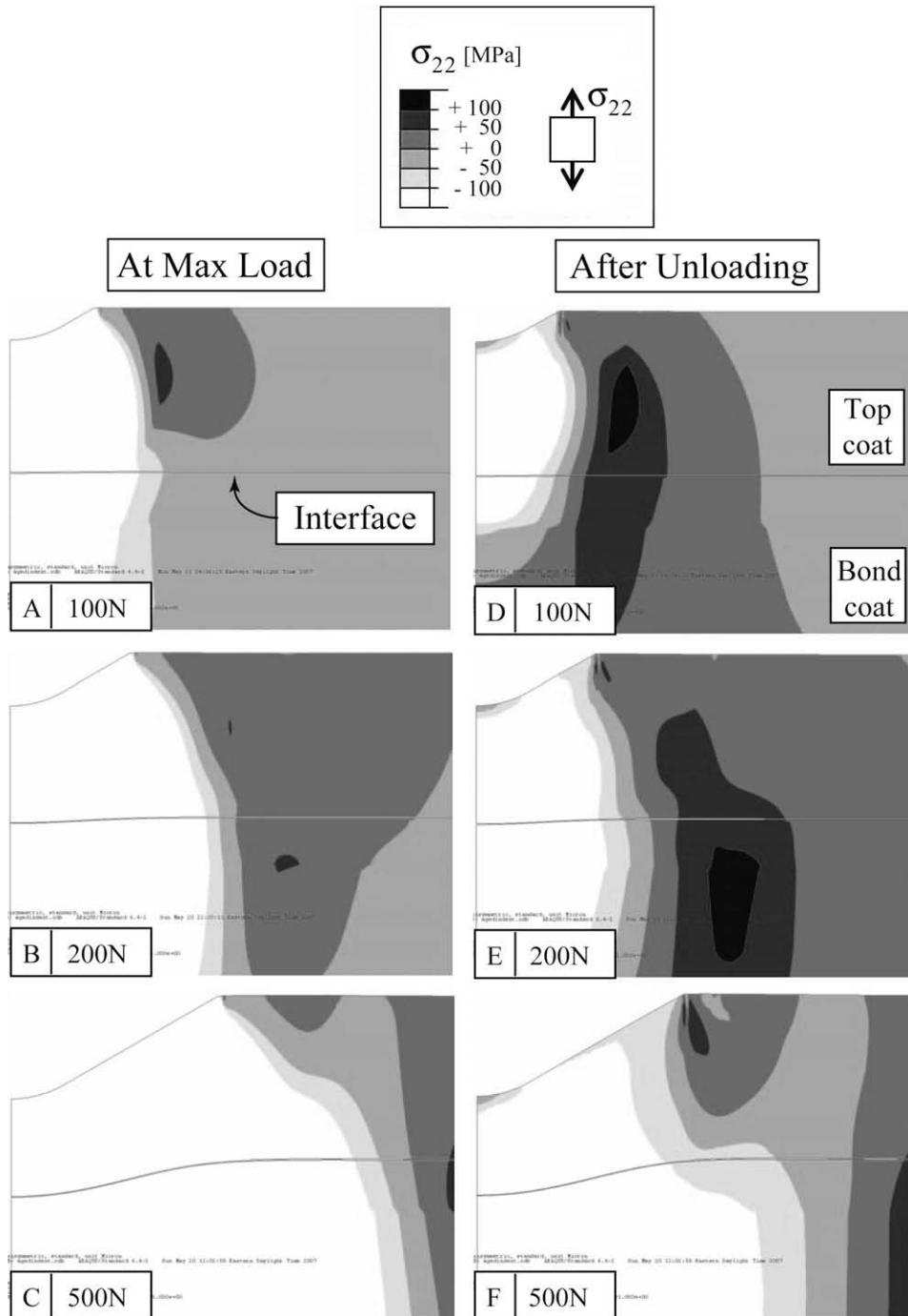


Fig. 6. Out-of-plane stresses (σ_{22}) for homogeneous top coat at maximum load (left column) and after unloading (right column), for maximum indentation forces of 100, 200, and 500 N (top to bottom). Hundred hours of aged conditions assumed (Tables 1 and 2).

For the homogeneous top coat, we use the properties obtained for the top coat columns (see Tables 1 and 2). This results in a slightly stiffer loading response, not shown for brevity.

The properties of the bond coat and the substrate remain constant for all models, and their elastic modulus are set to 200 GPa. The yield strength of the bond coat is 300 MPa and the substrate is assumed to remain elastic.

The indentation is simulated by using a prescribed deformation, since this is numerically easier to perform. However, to compare with the experimental observations, we need to compare the three cases as-coated, 50 h and 100 h for the same applied maximum

force. Thus, for a given force, we indent the structure until the desired force is reached, and then unload the structure.

Even though a model including the cracks (and propagation of the crack tip along with remeshing each time-step) is the only way to establish the true fracture behavior, we will here only investigate the stress fields that results from the indentation testing. This will give important information about the behavior of the highly non-linear system, without the need for time consuming calculations involving cracks. As will be seen from the results, the stress fields are very sensitive to the loading conditions and the properties.

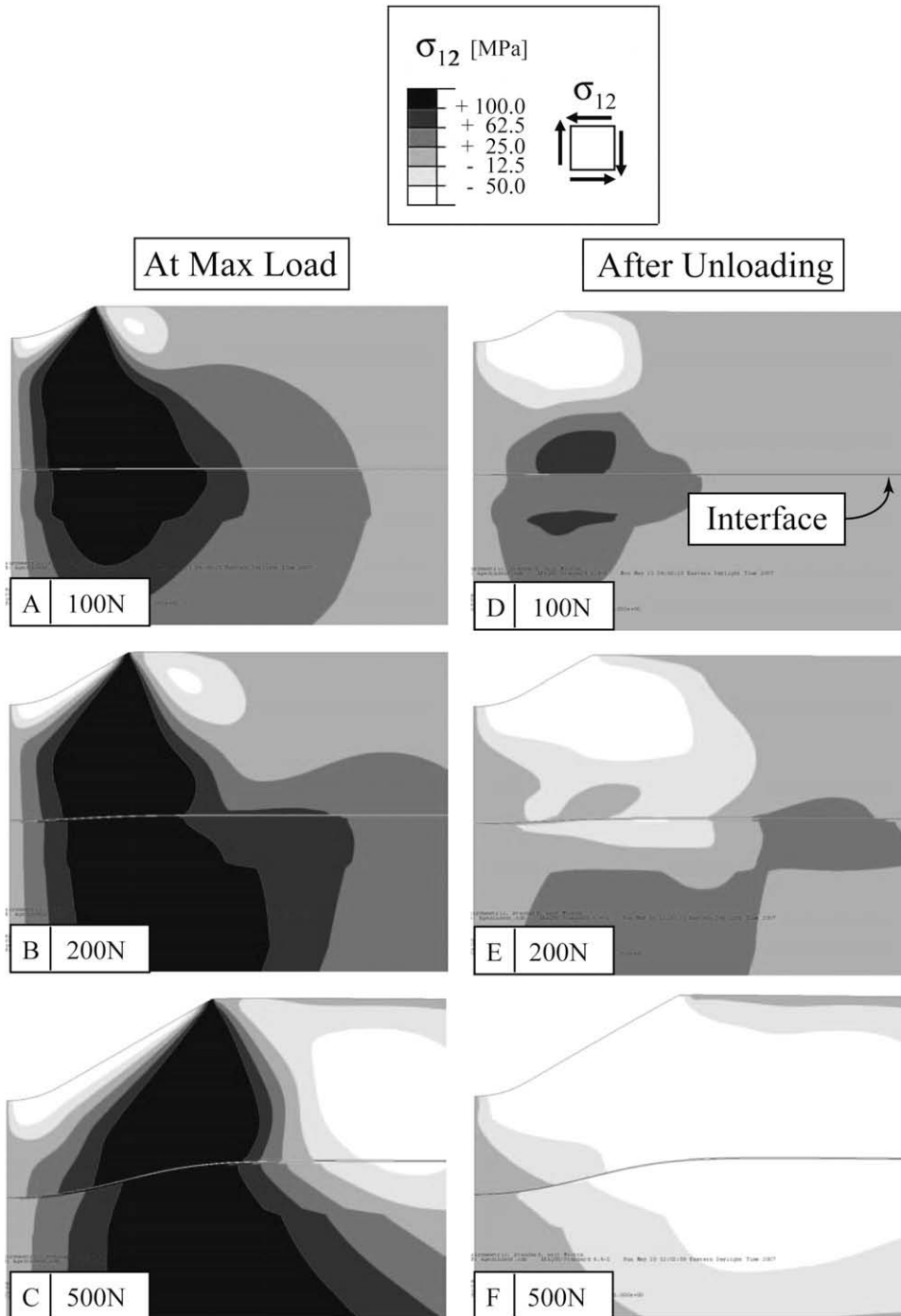


Fig. 7. Shear stresses (σ_{12}) for homogeneous top coat at maximum load (left column) and after unloading (right column), for maximum indentation forces of 100, 200, and 500 N (top to bottom). Hundred hours of aged conditions assumed (Tables 1 and 2).

4. Results and discussion

As mentioned previously, we will conduct a qualitative assessment of the mechanical response due to the indentation in the multilayered coating. To this end, we will focus on the stresses that develop during the indentation, including the residual stress field after unloading.

We will first consider the case of a homogeneous top coat. Since we are primarily interested in the delamination (interface) cracks that are induced by the indentation, we investigate two stress components. We will refer to these stress components as “out-

of-plane” stress (associated with mode I at the interface), σ_{22} , shown in Fig. 6, and “shear stress” (associated with mode II at the interface), σ_{12} , as shown in Fig. 7. In these figures, we show the stresses for when the indentation has reached its maximum indentation force (left column) and the residual stress fields after unloading (right column).³ Three cases are considered: ranging from low to large maximum indentation force: 100, 200, and 500 N,

³ “Maximum indentation force” refers to the maximum force achieved before unloading. The stress field obtained for different maximum indentation forces are NOT self-similar in a coated structure, which will be discussed in the following.

assuming the properties for 100 h aged specimens (see Tables 1 and 2). It is evident that the stress fields developed at maximum indentation load and after unloading increase in accordance with the increase of the maximum indentation force, as may be expected. However, based on these stress fields, it is not evident how to explain the classification of the delamination diameter into “small” and “large” indentation load, as was implied in Fig. 3.

Thus, we will investigate if the columnar structure of the top coat can lead to the bifurcation of interfacial crack diameter as suggested by Fig. 3. A parallel scenario to the homogeneous top coat is investigated; three levels of maximum indentation force (100, 200, and 500 N) are considered in Fig. 8 (σ_{22}) and Fig. 9 (σ_{12}). A signif-

icant difference between the stress fields is observed when the individual columns in the top coat are modeled compared to the homogeneous top coat, particularly after unloading. For the lower maximum indentation force, Fig. 8D, a relatively high tensile out-of-plane stress develops after unloading in the interface, directly beneath the indented area. This high tensile stress of about 300 MPa may be large enough to drive a crack. This is not observed for the homogeneous bond coat (Fig. 6D). For the cases of higher maximum indentation force, the unloaded stress state shows that the stress level decreases in the interface under the indenter and vanishes at the higher indentation forces (Fig. 8E and F). For the highest maximum indentation forces (500 N), Fig. 8F, two tensile

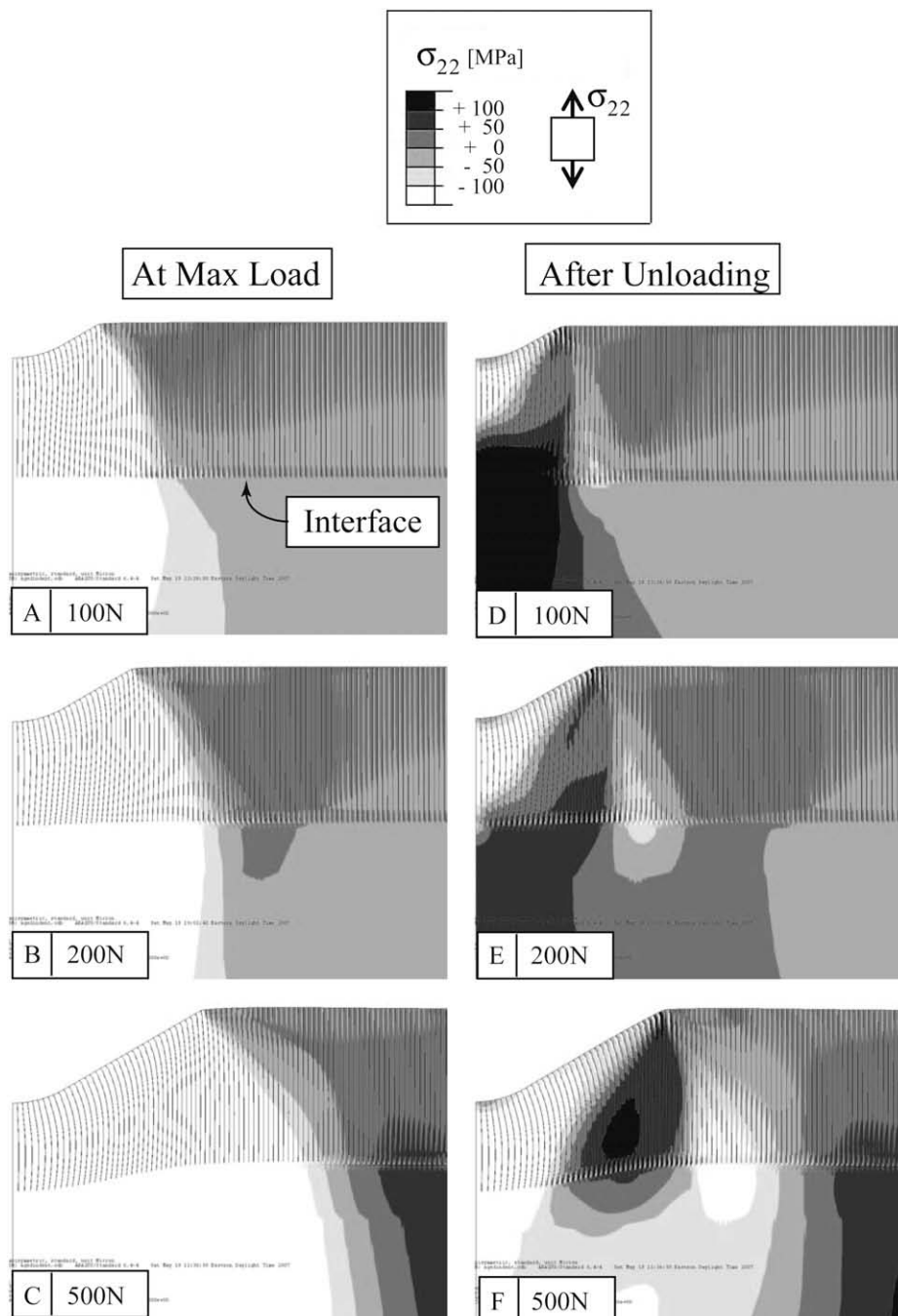


Fig. 8. Out-of-plane stresses (σ_{22}) for columnar top coat at maximum load (left column) and after unloading (right column), for maximum indentation forces of 100, 200, and 500 N (top to bottom). Hundred hours of aged conditions assumed (Tables 1 and 2).

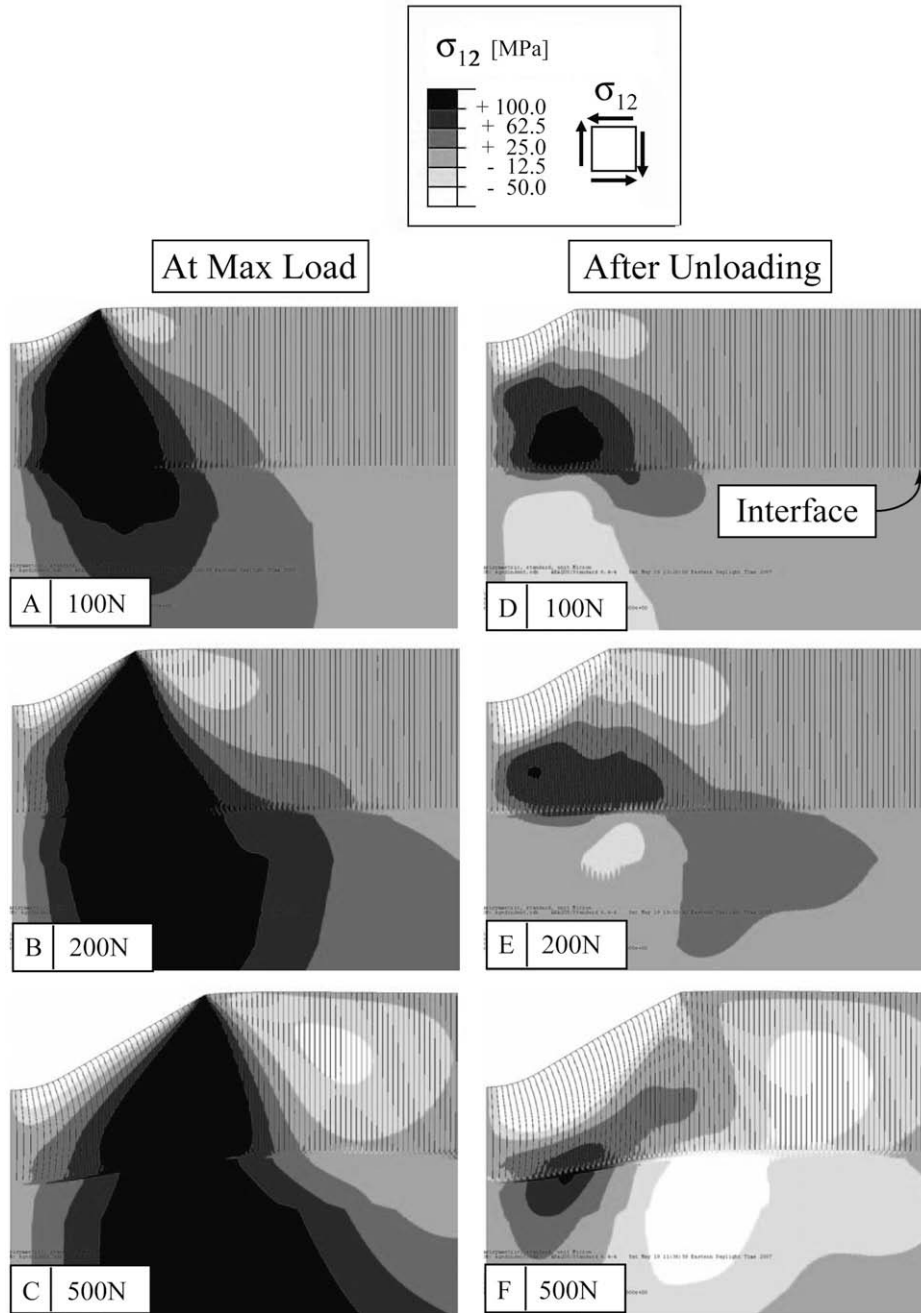


Fig. 9. Shear stresses (σ_{12}) for columnar top coat at maximum load (left column) and after unloading (right column), for maximum indentation forces of 100, 200, and 500 N (top to bottom). Hundred hours of aged conditions assumed (Tables 1 and 2).

regions are observed during unloading in the interface, one at the periphery of the indentation and one further out, away from the center of the indentation.

In order to quantify the interfacial stresses, we plot the stresses in the interfacial region of the samples with columnar top coat as a function of the radius, R , as defined in Fig. 4. The interface we are concerned with is not one interface, but at least three interfaces: (i) the interface between the top coat and the TGO; (ii) the interface between the initial (porous) TGO and the newly grown TGO; and (iii) the interface between the TGO and the bond coat (see Figs. 1 and 4). By plotting the tensile and shear stresses at these three interfaces (extracted from the nodal points), we see that the stresses have similar nominal values (for each of the cases considered), in particular for the normal stress, σ_{22} , Fig. 10. The shear stress has

a slightly higher discrepancy, but we believe that the normal stress will in general be the dominating stress component for debonding. Moreover, the interface between the TGO and the bond coat does not have the highly, locally fluctuating stresses as the other two layers have. These local fluctuations are associated with the columnar structure and may or may not be real (may be an artifact of the discrete nature of the numerical model associated with the ICS). Thus, for simplicity we will in the following only display the stresses at the interface between the TGO and the bond coat.

When investigating the interfacial stresses for various maximum indentation forces, the differences between homogeneous and columnar structures are clearly seen, Fig. 11. The residual interfacial tensile stresses after unloading in the case of homogeneous top coat all have similar maximum value, independent of

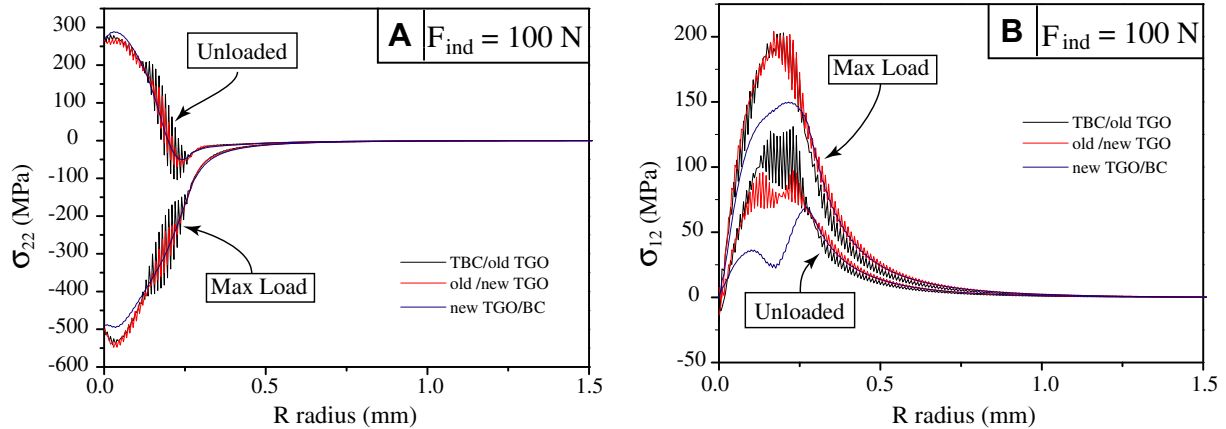


Fig. 10. The interfacial stresses (A) tensile stress and (B) shear stress, for 100 N maximum indentation force for the three interfaces. Columnar top coat, 100 h aged conditions assumed (Tables 1 and 2).

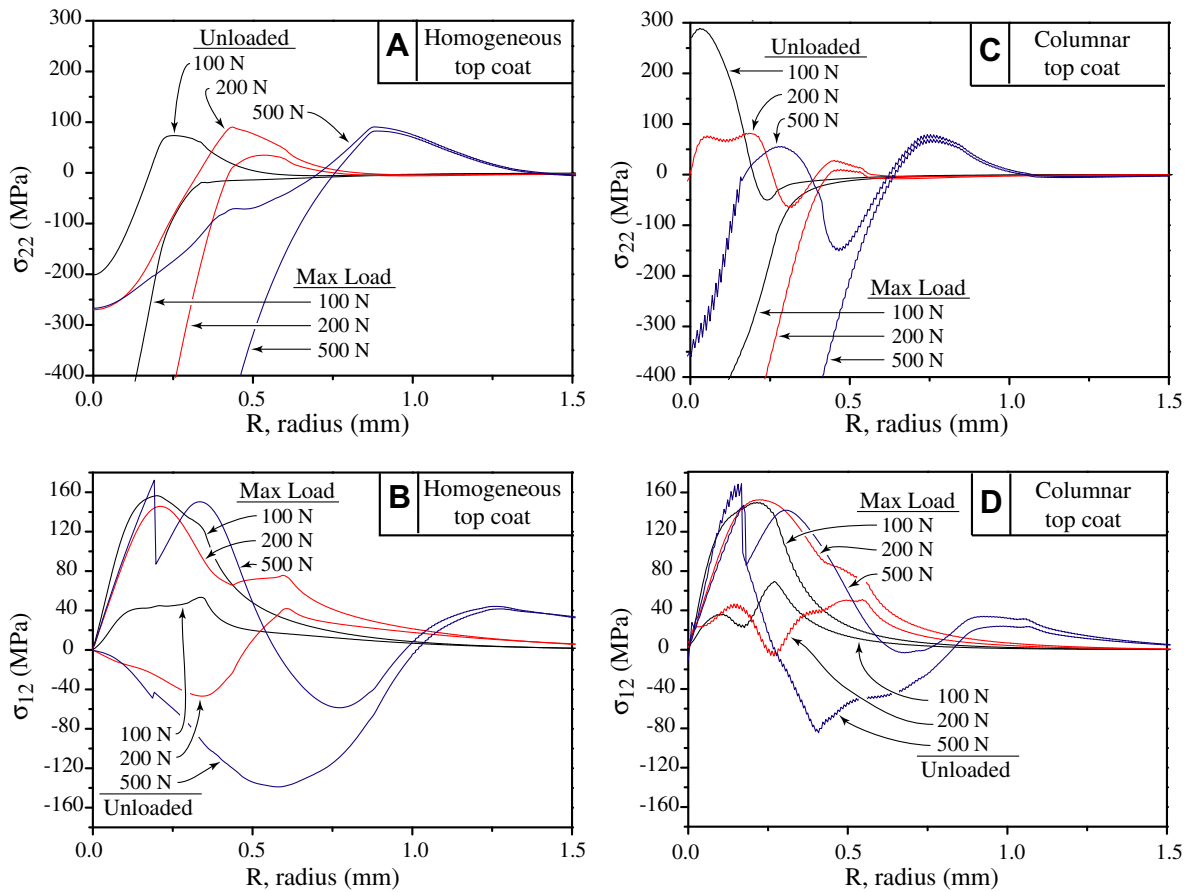


Fig. 11. The interfacial stresses for maximum indentation forces of 100, 200, and 500 N: (A) tensile stress and (B) shear stress for the homogeneous top coat; (C) tensile stress and (D) shear stress for the columnar coat. TGO–bond coat interface, 100 h aged conditions assumed (Tables 1 and 2).

the maximum indentation force. However, for the investigated range of maximum indentation forces, the tensile regions move outwards, towards higher radii with increasing maximum indentation force, Fig. 11A. For the case of columnar top coat, the tensile region appears directly underneath the indentation for lower maximum indentation forces, and the magnitude is significantly higher for the lower loads (for the investigated range of indentation loads), Fig. 11C. In fact, for the case of 100 N maximum indentation force, the residual tensile stress is about three times as high as the peak stress for the homogeneous top coat (Fig. 11C). When maxi-

imum indentation forces smaller 100 N were explored, we found that 70 N appears to result in the highest peak tensile stress at the interface, Fig. 12. As the maximum indentation force is increased, the magnitude of the tensile stress is reduced and the distribution is changed (Fig. 11C). For the highest maximum indentation load (500 N), two tensile regions are observed after unloading. Thus, the lower maximum indentation forces result in a “peak” residual tensile stress directly beneath the imprinted area, supporting the notion that the behavior for lower maximum indentation forces is different from the response of higher maxi-

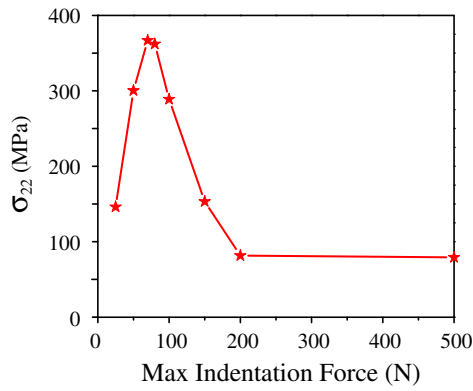


Fig. 12. Peak interfacial tensile stress as a function of maximum indentation force. 100 h aged conditions assumed (Tables 1 and 2). The stars symbolizes calculated values, the lines are “guide-for-the-eye.”

imum indentation loads. In addition, the interfacial shear stresses also contribute to interfacial fracture, and only the magnitude is important. From Fig. 11B and D it may be seen that the shear stresses in the interface exhibit a more complex behavior when the columnar structure is modeled, but the overall magnitudes are not significantly different. In all, the results show that there is a fundamental change between “small” and “large” maximum indentation force (Fig. 11C), supporting the notion of a bifurcation in the response, as suggested in Fig. 3.

Moreover, in the thermography experiments conducted in the companion paper [6], it was seen that cracks grow during loading. The numerical simulations show that for larger maximum indentation forces, the stress field indeed encourages crack growth during loading, but not for smaller maximum indentation loads [6] where interfacial tensile stresses appear during unloading.

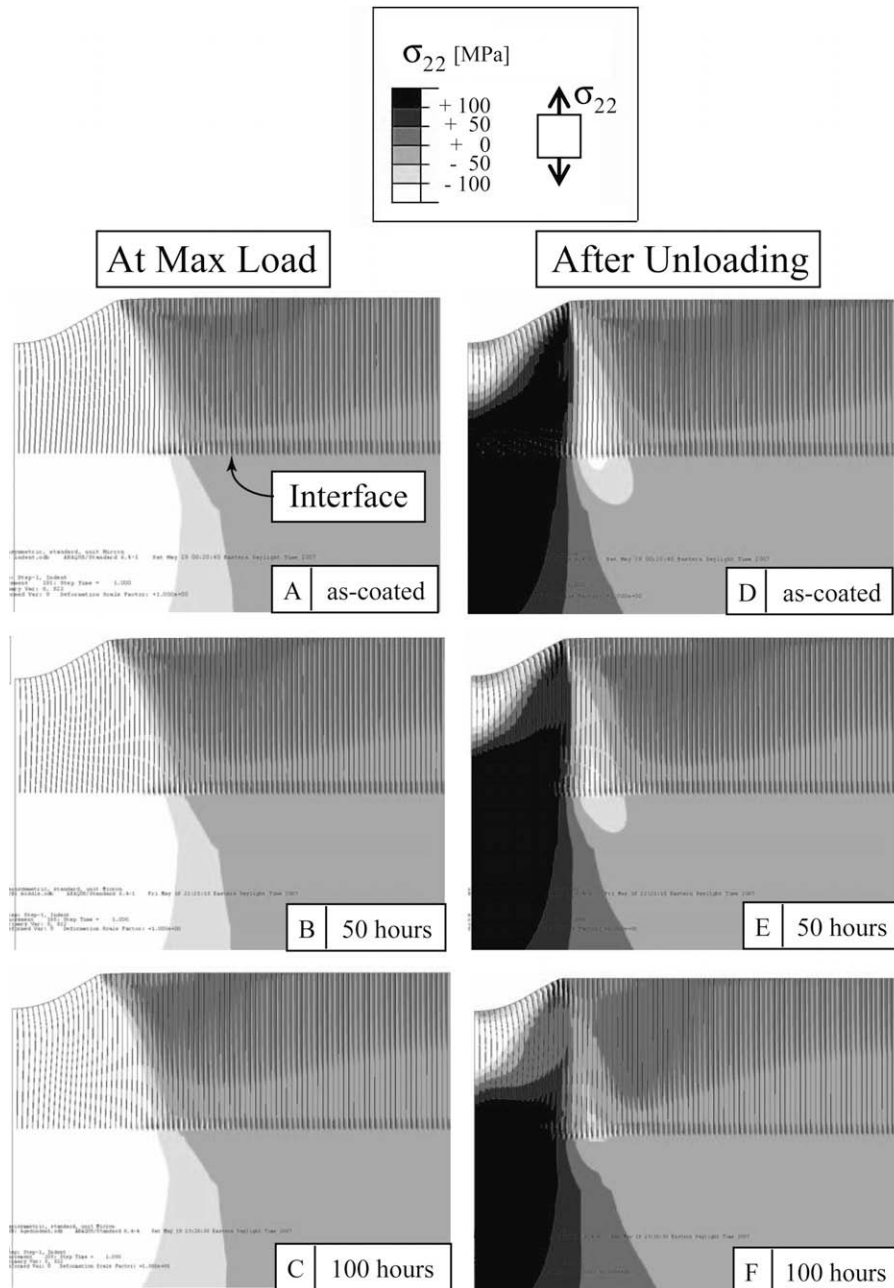


Fig. 13. For the case of indentation force 100 N, out-of-plane stresses (σ_{22}) for columnar top coat at maximum load (left column) and after unloading (right column). As-coated, 50 h, and 100 h aged (top to bottom).

Lastly, we will investigate if the numerical simulations support the experimentally observed difference between aged and as-coated samples as shown in Fig. 3, where – for a given load – the as-coated samples show a larger delamination than the aged samples. The age of the samples is simulated as discussed in Section 3 with the properties summarized in Tables 1 and 2, corresponding to as-coated, 50 h and 100 h aged. We will investigate two load levels: “low” and “high” maximum indentation load, quantified with the maximum indentation forces 100 N and 500 N, respectively. The stress contour plots are shown in Figs. 13 and 14 and the interfacial stresses in Fig. 15. The effect of aging is primarily seen in the overall response of the out-of-plane stress (σ_{22}) and in particular

for the lower indentation load (Fig. 13D–F). Even though the higher indentation loads, as well as the shear stresses, are influenced by the age of the system, the differences are not as evident within the resolution of the contour plots. Interestingly, if the stresses in the interface alone are considered, Fig. 15, the σ_{22} components for both 100 N and 500 N maximum indentation force (Fig. 15 and C, respectively), show only minor differences, respectively. These differences are small enough that for the qualitative analyses pursued here, the numerical simulations do not directly support the experimental differences, Fig. 3. Thus, the differences must stem from the material strength (fracture resistance), which is not captured in the current model.

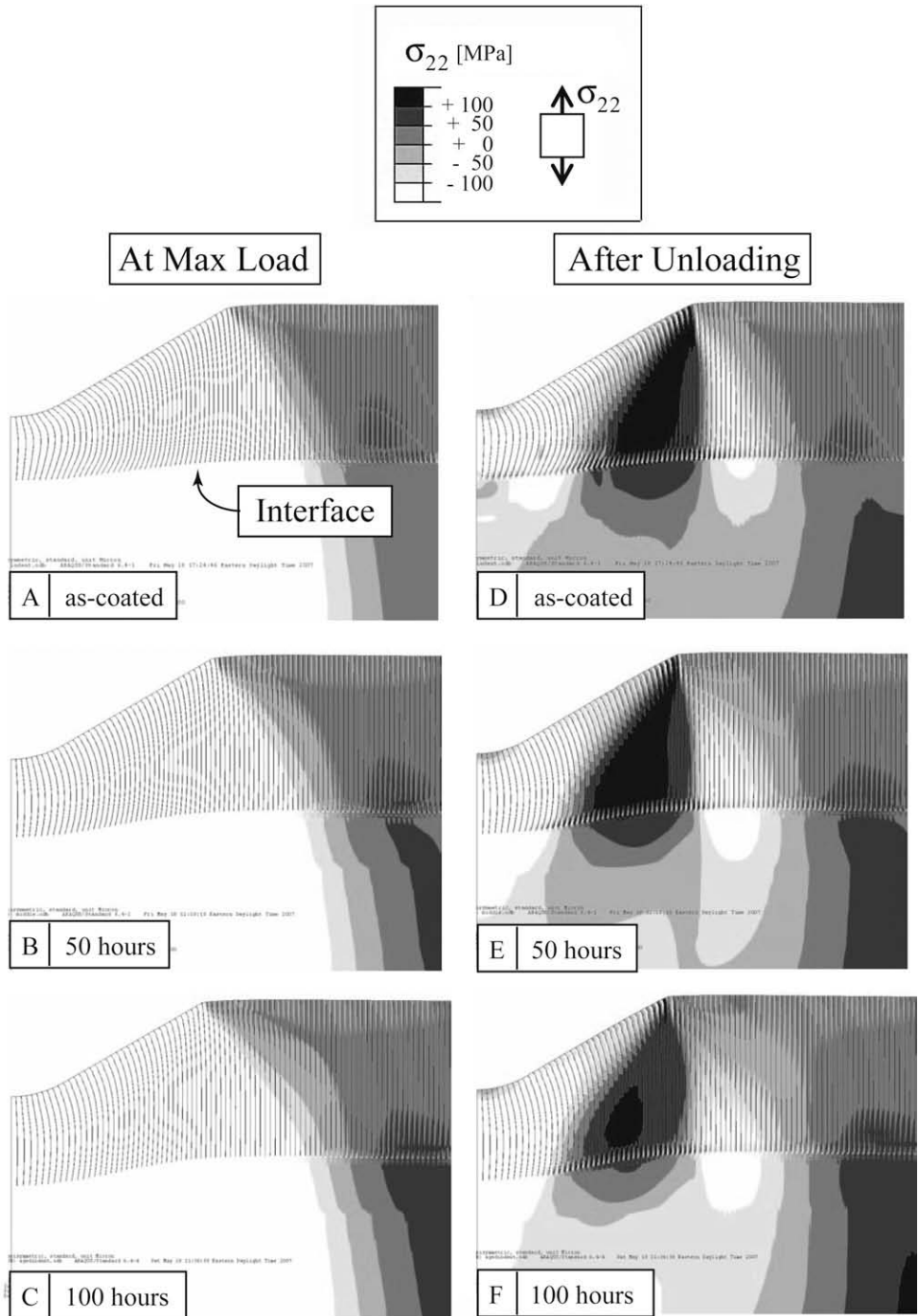


Fig. 14. For the case of indentation force 500 N, out-of-plane stresses (σ_{22}) for columnar top coat at maximum load (left column) and after unloading (right column). As-coated, 50 h, and 100 h aged (top to bottom).

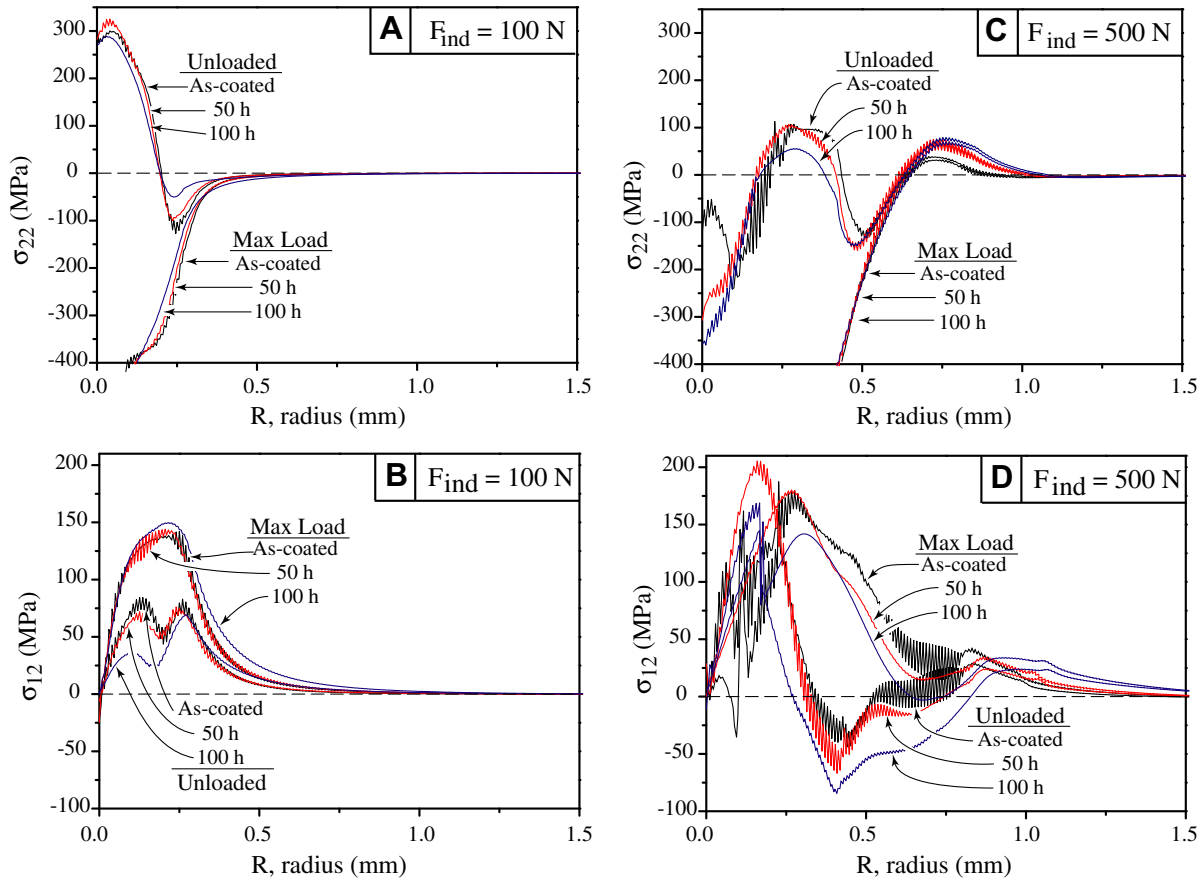


Fig. 15. The interfacial stresses for as-coated, 50 h and 100 h aged specimens. Maximum indentation force 100 N (A) tensile stress and (B) shear stress; and for 500 N (C) tensile stress and (D) shear stress. Columnar coat, TGO–bond coat interface.

We believe that the ambiguous results seen in the experimental investigations derives from that the delaminations did not occur at the weakest interface for the aged specimens: as discussed in Section 2, the indentation tends to result in interfacial cracks that propagate in the mixed and porous TGO and in the YSZ, whereas the spontaneous delaminations that occurred (400 h aged samples spalled spontaneously and 200 h spalled at a later time, “desk-top effect”) were primarily between the dense TGO and the bond coat. To capture this, the model needs to be improved to incorporate crack growth at different interfaces, which will be the objectives for a future study.

5. Concluding remarks

In this study, the response from using Rockwell indentation as a means of establishing the interfacial fracture toughness in thermal barrier coatings (TBCs) was explored by numerical simulations. Previous experimental investigations showed that the results obtained were ambiguous and appeared to be contradictory. By measuring the size of the interfacial delamination as a function of the maximum indentation force, the experimental data indicated that (i) the delamination response can be divided into two branches; one response for “small” indentation loads and one for “large” indentation loads, and (ii) the samples aged at high temperature before indentation testing gave the contradictory results of shorter cracks than the as-coated samples. In this work, we elucidate some of these observations through finite element analysis.

The simulations showed that it is important to simulate the columnar structure of the ceramic top coat. A homogeneous top

coat does not support the experimentally obtained bifurcation between “small” and “large” indentation loads. However, this division can be seen from models containing a columnar top coat. For smaller maximum indentation forces, a large tensile stress develops underneath the indented region after unloading, suggesting that the crack may grow during unloading. However, for larger maximum indentation forces, tensile stresses develop during loading at the interface, facilitating crack growth during loading. In addition, for a given top coat column width, different maximum indentation forces (or depths) lead to different bending deformation of top coat columns, thus causing distinct influence zones via columnar interactions. We believe that this explains the experimentally observed behavior where small indentation loads result in a different behavior of the delamination crack than when larger indentation loads are imposed.

A relatively small difference between the stresses at the TGO–bond coat interface due to aging is observed numerically, primarily because the column bending behavior is less affected by the relatively minor adjustments of material properties with aging. Thus, we believe that the experimentally observed discrepancy is due to the toughness change of the TGO-system due to ageing. Experimentally, it is observed that for the aged specimens, the delamination crack did not occur at the weakest interface: as discussed in our experimental work [6], the true weakest link is the interface between the bond coat and TGO (this is where the spontaneous failures occur). However, the indentation induced cracks primarily near the interface between the top coat and the TGO, and in the preexisting TGO (the TGO formed during processing). The cracks were not able to penetrate through the dense TGO (formed during aging). This model did not include the crack propagation and was

therefore not able to capture this behavior. The more detailed model simulating the crack growth is left for a future study.

Consequently, indentation may not be a suitable method for measuring the “weakest link” interfacial fracture toughness for thermal barrier coatings, which is the value that must be considered when designing the coating. Since the limitation appears to be caused by a “strong” layer (the dense TGO) that prevents the crack from penetrating to the weakest interface, these observations may have implication for other multilayered structures as well: the delamination crack may not propagate in the weakest interface if a layer with high fracture toughness prevents the cracks from developing there. Thus, careful analysis must be done when measuring the interfacial fracture toughness of multilayered structures.

Acknowledgements

The authors acknowledge the financial support by the National Science Foundation, DMR-0346664 and the Office of Naval Research ONR-N00014-04-1-0498 (JY and AMK), the European Community's Human Potential Program under contract HPRN-CT-2002-00203 [SICMAC] (MB), and NSF CMS-0407743 (XC).

References

- [1] L.L. Shaw, B. Barber, E.H. Jordan, M. Gell, *Scripta Materialia* 39 (1998) 1427–1434.
- [2] J.A. Ruud, A. Bartz, M.P. Borom, C.A. Johnson, *Journal of the American Ceramic Society* 84 (2001) 1545–1552.
- [3] J. Aktaa, K. Sfar, D. Munz, *Acta Materialia* 53 (2005) 4399–4413.
- [4] A. Vasinonta, J.L. Beuth, *Engineering Fracture Mechanics* 68 (2001) 843–860.
- [5] M. Bartsch, B. Baufeld, in: *Proceedings of the European Conference on Fracture – ECF 14 I*, 2002, p. 209.
- [6] J. Yan, T. Leist, M. Bartsch, A.M. Karlsson, *Acta Materialia* 56 (2008) 4080–4090.
- [7] M. Bartsch, I. Mircea, J. Suffner, B. Baufeld, *Key Engineering Materials* 290 (2005) 183–190.
- [8] U. Schulz, M. Menzebach, C. Leyens, Y.Q. Yang, *Surface and Coatings Technology* 146 (2001) 117–123.
- [9] S.Q. Guo, D.R. Mumm, A.M. Karlsson, Y. Kagawa, *Scripta Materialia* 53 (2005) 1043–1048.
- [10] H.A. Bahr, H. Balke, T. Fett, I. Hofinger, G. Kirchhoff, D. Munz, A. Neubrand, A.S. Semenov, H.J. Weiss, Y.Y. Yang, *Materials Science and Engineering A-Structural Materials Properties Microstructure and Processing* 362 (2003) 2–16.
- [11] Q. Ma, Ph.D. thesis: *Indentation Methods for Adhesion Measurement in Thermal Barrier Coating Systems*, in: Carnegie Mellon University, Pittsburgh, 2004.
- [12] M.R. Begley, D.R. Mumm, A.G. Evans, J.W. Hutchinson, *Acta Materialia* 48 (2000) 3211–3220.
- [13] Y.H. Sohn, B. Jayaraj, S. Laxman, B. Franke, A.M. Karlsson, *Journal of Materials (JOM)* (2004) 53–57.
- [14] ABAQUS, ABAQUS 6.5, ABAQUS Inc., Pawtucket, Rhode Island, 2004.
- [15] X. Chen, J.W. Hutchinson, A.G. Evans, *Acta Materialia* 52 (2004) 565–571.
- [16] X. Chen, *Surface and Coatings Technology* 200 (2006) 3418–3427.
- [17] A.L. Gurson, *Journal of Engineering Materials and Technology-Transactions of the ASME* 99 (1977) 2–15.
- [18] S.D. Mesarovic, N.A. Fleck, *Proceedings of the Royal Society of London A455* (1999) 2707–2728.